Author(s): Li, Jibo; Li, lixuan; Bhaskar, Bichu; Toivanen, Ville; Tarvainen, Olli; Hitz, Denis; Li, Libin; Lu, Wang; Koivisto, Hannu; Thuillier, Thomas; Guo, Junwei; Zhang, Xuezhen; Zhao, Huanyu; Sun, Lingting; Zhao, Hongwei

Title: Effects of magnetic configuration on hot electrons in a minimum-B ECR plasma

Year: 2020

Version: Accepted version (Final draft)

Please cite the original version:

Li, J., Li, L., Bhaskar, B., Toivanen, V., Tarvainen, O., Hitz, D., Li, L., Lu, W., Koivisto, H., Thuillier, T., Guo, J., Zhang, X., Zhao, H., Sun, L., & Zhao, H. (2020). Effects of magnetic configuration on hot electrons in a minimum-B ECR plasma. Plasma Physics and Controlled Fusion, 62(9), Article 095015. https://doi.org/10.1088/1361-6587/ab9d8f

ACCEPTED MANUSCRIPT

Effects of magnetic configuration on hot electrons in a minimum-B ECR plasma

To cite this article before publication: Jibo Li *et al* 2020 *Plasma Phys. Control. Fusion* in press https://doi.org/10.1088/1361-6587/ab9d8f

Effects of magnetic configuration on hot electrons in a minimum-B ECR plasma

J. B. Li[1], L. X. Li[1,2], B. S. Bhaskar[3,4], V. Toivanen[3], O. Tarvainen[3,5], D. Hitz[1], L. B. Li[1], W. Lu[1], H. Koivisto[3], T. Thuillier[4], J. W. Guo[1], X. Z. Zhang[1,2], H. Y. Zhao[1,2], L. T. Sun[1,2;a)] and H. W. Zhao[1,2]

[1]*Institute of Modern Physics (IMP), Chinese Academy of Sciences, Lanzhou 730000, China*
[2]*School of Nuclear Science and Technology, University of Chinese Academy of Sciences, Beijing 100049, China*
[3]*University of Jyväskylä, Department of Physics, PO Box 35 (YFL), 40500 Jyväskylä, Finland*
[4]*Laboratoire de Physique Subatomique et de Cosmologie, 53 avenue des Martyrs, 38026 Grenoble Cedex, France*
[5]*STFC ISIS Pulsed Spallation Neutron and Muon Facility, Rutherford Appleton Laboratory, Harwell, OX110QX, UK*

a) E-mail: sunlt@impcas.ac.cn

Abstract

To investigate the hot electron population and the appearance of kinetic instabilities in highly charged electron cyclotron resonance ion source (ECRIS), the axially emitted bremsstrahlung spectra and microwave bursts emitted from ECRIS plasma were synchronously measured on SECRAL-II (Superconducting ECR ion source with Advanced design in Lanzhou No. II) ion source with various magnetic field configurations. The experimental results show that when the ratio of the minimum field to the resonance field (i.e. B_{min}/B_{ecr}) is less than ~0.8, the bremsstrahlung spectral temperature T_s increases linearly with the B_{min}/B_{ecr}–ratio when the injection, extraction and radial mirror fields are kept constant. Above this threshold T_s saturates and the electron cyclotron instability appears simultaneously. This study has also demonstrated that T_s decreases linearly with the increase of the average gradient over the ECR surface when the on-axis gradient and hexapole field strengths are constant. In addition, it is found that T_s decreases with the increase of the gradient at the resonance zone (∇B_{ecr} on axis and $<\nabla B_{ecr}>$) at relatively low mirror ratio and is insensitive to the gradient at high mirror ratio when B_{min} is constant. Compared to a recent study taken on a fully superconducting ECRIS (Benitez et al. 2017 *IEEE Trans. Plasma Sci.* **45** 1746-54), in which it was concluded that T_s is only sensitive with B_{min}, this article shows different results discussing the mechanisms behind the correlation of magnetic field parameters to T_s.

1. Introduction

Electron cyclotron resonance (ECR) ion sources are used to produce a wide range of ions, from singly charged to multiply charged ions (MCIs) and have been widely applied to both basic and applied scientific research due to their efficiency and reliability [1, 2]. In the past decades, a series of well performing ECR ion sources were developed at the Institute of Modern Physics (IMP) [3-10] and continuous efforts were spent to deepen the understanding of the plasma mechanisms involved in these ion sources and thereby to further improve their performances [11-16].

The plasmas in modern ECRISs are commonly confined in a so-called minimum-B field which is a superposition of solenoid and sextupole fields. Electrons in the plasma are heated by the process of electron cyclotron resonance that takes place where the electron cyclotron frequency is approximately equal to the injected microwave frequency. MCIs are created through stepwise electron impact ionization by the electrons heated in the ECR. However, hot electrons, with energies of several hundreds of keV or more should be avoided as they do not contribute significantly on the ionization process but can add a significant heat load to the cryostat of modern superconducting ECRISs through absorption of wall bremsstrahlung photons [17, 18]. Meanwhile, it has been shown that [19-21] ECR plasmas are prone to electron cyclotron instabilities driven by hot electrons with strongly anisotropic electron velocity distribution (EVD), which will lead to ms-scale oscillation of the extracted beam current.

This article deals with experimental studies of the hot electron population of a highly charged ECR ion source. As collisions between electrons and ions within the plasma volume lead to bremsstrahlung radiation, the analysis of bremsstrahlung spectra is a powerful diagnostic tool for studying the hot electron population [22, 23] and can also be used to probe the electron heating mechanism in ECR produced plasmas, from compact all-permanent magnet [24] to large fully superconducting devices [13, 25]. To compare our results with previous articles published on the same subject, bremsstrahlung measurement was chosen to diagnose the plasma of SECRAL-II ion source. Meanwhile, since the electron cyclotron instabilities are driven by hot electrons interacting resonantly with electromagnetic plasma waves, the measurement of characteristic microwave emission emitted from the ECRIS plasma can be used as a direct plasma instability diagnostics method [19] and was also employed in this study to investigate the appearance of electron cyclotron instabilities.

A number of previous studies taken on ECRISs [13, 25-27] show that the magnetic field configuration is extremely important for the production of hot electrons in minimum-B topology. Although these earlier studies showed important results, the mechanism behind the correlation of magnetic field parameters to the bremsstrahlung spectral temperature T_s is not yet clear. Furthermore, it has been demonstrated that the most critical ion source tuning parameter affecting the appearance of electron cyclotron instabilities and beam current oscillations is the magnetic field [19], but the possible correlation between bremsstrahlung spectra and the appearance of electron cyclotron instabilities are still unknown. Therefore, to further investigate the effects of magnetic configuration on hot electrons in a minimum-B ECR plasma, in this paper we present a detailed experimental study of the hot electron population through synchronous measurements of plasma bremsstrahlung and instability-induced microwave signal in a much wider range of magnetic configurations than those presented in previous articles (including the so-called turbulent region where instabilities occur). The experimental setup and equipment are described in section 2; in section 3, the experimental results are reported; a discussion about the data is then shown in section 4, followed by the conclusions in section 5.

2. Experimental setup

2.1 SECRAL-II ion source

SECRAL-II ion source has been successfully designed and developed at IMP [28]. This ion source is a third generation ECR machine optimized for the operation at 18, 24 and 28 GHz. The superconducting magnet assembly of SECRAL-II (shown in Figure 1) consists of three axial solenoid coils and a sextupole to generate the minimum-B magnetic field configuration. The magnetic field profile is typically 3.7 T at the injection, 2.2 T at the extraction with a radial field of 2.0 T at the Ø125 mm chamber wall. As the source magnet is fully superconducting, SECRAL-II has the flexibility of easily varying the magnetic structure by independently changing the injection field, B_{inj}, the extraction field, B_{ext}, the minimum-B value, B_{min} and the radial field, B_r, so that one can investigate the effect of magnetic field configuration in detail.

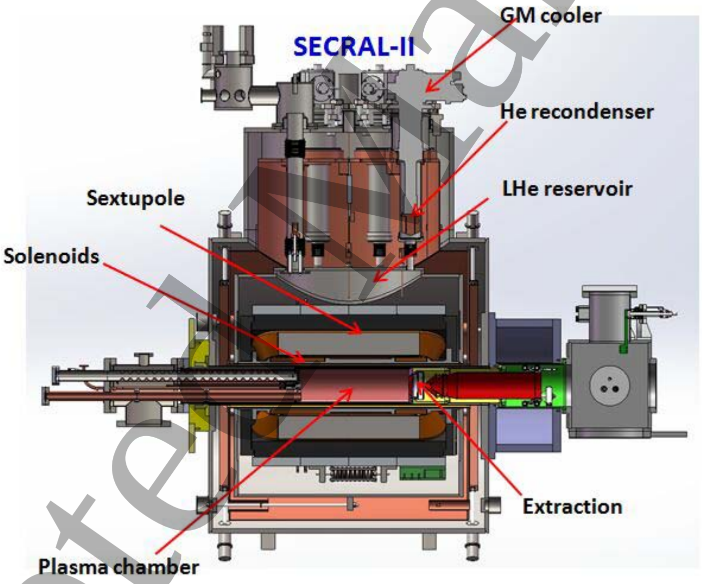

Figure 1: Layout of the SECRAL-II ion source.

2.2 Bremsstrahlung detection system and spectral temperature T_s determination

As SECRAL-II is fully superconducting, the only possibility to install a diagnostic is on a line-of-sight through the source axis. The axially emitted bremsstrahlung spectra from SECRAL-II are measured with an Amptek XR-100T-CdTe detector and PX5 digital pulse processor [29] through an Al window located at the end of the straight-through port of the beam analyzing magnet (shown in Figure 2). The detector is a semiconductor type with a detection efficiency of 10% or greater in the energy range of 10 to 300 keV and is placed behind the straight-through port. In order to focus on the center of the plasma and prevent wall bremsstrahlung interfering with the detection system, a lead collimation system is designed with MCNP (Monte Carlo N-Particle Transport Code) [30, 31] and is set up between the straight-through port and the detector. In addition, an X-ray blocking made of tantalum (diameter: 30 mm, thickness: 20 mm) is installed on the optical axis, it blocks the X-rays from entering the collimation system and reaching the detector when inserted. The measurement solid angle is restricted to 6.7E-8 sr and the energy calibration of the spectrum is done using standard radioactive sources with known gamma lines. It is acknowledged that thick target bremsstrahlung emitted into backward angles from the biased disc located at the injection end of the ion source may contribute to the recorded spectra. Since the energy distribution of the electrons causing this contribution is unknown, it is impossible to estimate the ratio of the plasma bremsstrahlung and (biased disc) wall bremsstrahlung. However, as most of the radiation power from the biased disc is emitted into forward angles, and the area defined by the acceptance of the collimation system (Ø14 mm at the extraction aperture) includes only a small part of the extraction system, the main contribution to the bremsstrahlung spectra is therefore considered to be the plasma bremsstrahlung produced in the volume visible to the detector.

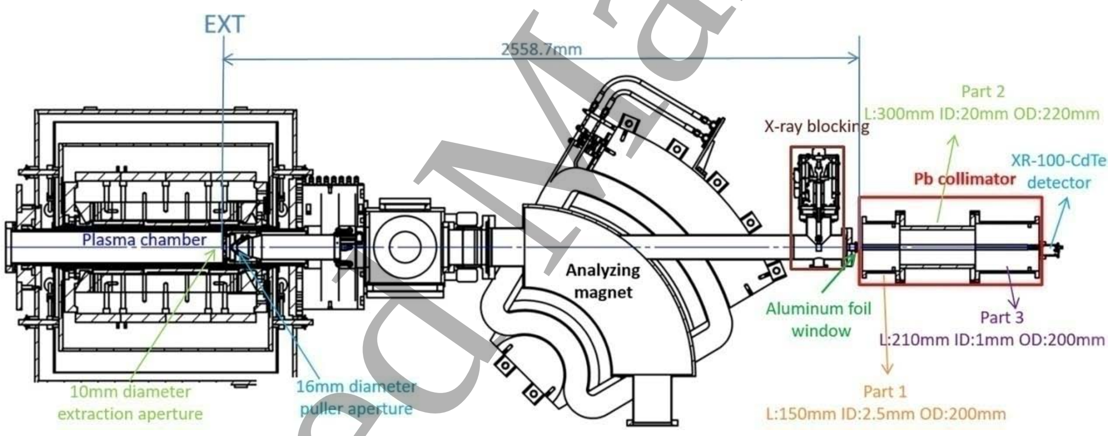

Figure 2: Bremsstrahlung detection system on SECRAL-II.

A parameter called the spectral temperature T_s is often used to characterize the bremsstrahlung spectra. T_s is inferred from the linear part of the semi-logarithmic representation of the recorded spectrum for which the spectral power $j(E) \propto \exp(-E/T_s)$, where *E* is the photon energy. We should note that this spectral temperature is not a direct measure of the temperature of the hot electrons, since the electron energy distribution in an ECRIS plasma is believed to be strongly non-Maxwellian [32]. This statement is supported by recent experiments measuring the energy distribution of electrons escaping from a minimum-B ECRIS [33]. For these reasons T_s must be regarded as qualitative measure of the hot electron (average) energy at best. Bearing these limitations in mind one can use T_s to study the influence of the external source parameters such as magnetic field strength, injected microwave power etc. on the hot electron population in relative terms. In our study, the bremsstrahlung spectra presented below are corrected by the detector efficiency and the spectral temperature T_s is obtained by the linear fit at the energy range 80–200 keV (shown in Figure 3).

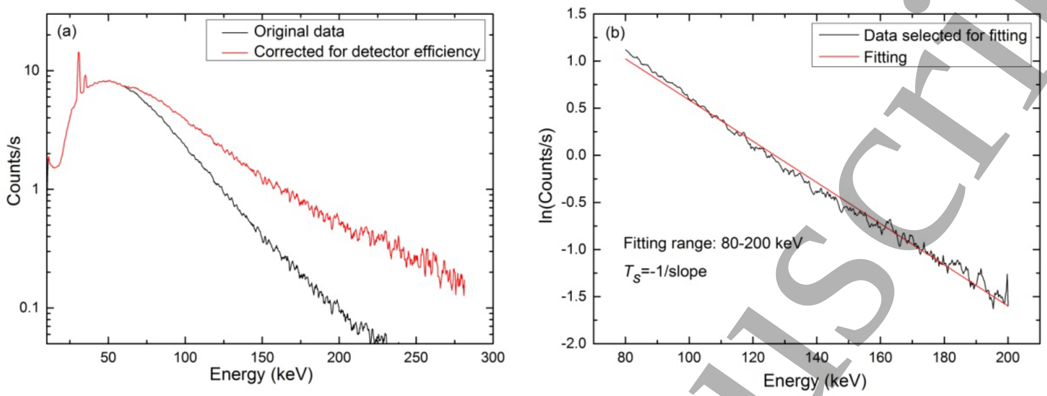

Figure 3: (a) Spectra corrected for detector efficiency. (b) A linear fitting of the semi-log plot of the data.

2.3 Microwave signal measurement and electron cyclotron instability

Figure 4 shows the experimental setup of the microwave signal measurement. A Low-Barrier Schottky Diode detector (0.01-26.5 GHz, 10 ns resolution) is connected to a WR-62 waveguide port at the injection of the ion source. The microwave signal emitted by the plasma is guided into oscilloscope through WR-62 waveguide port, high voltage break, waveguide-to-coaxial transition and adjustable attenuator (usually set to 20 dB).

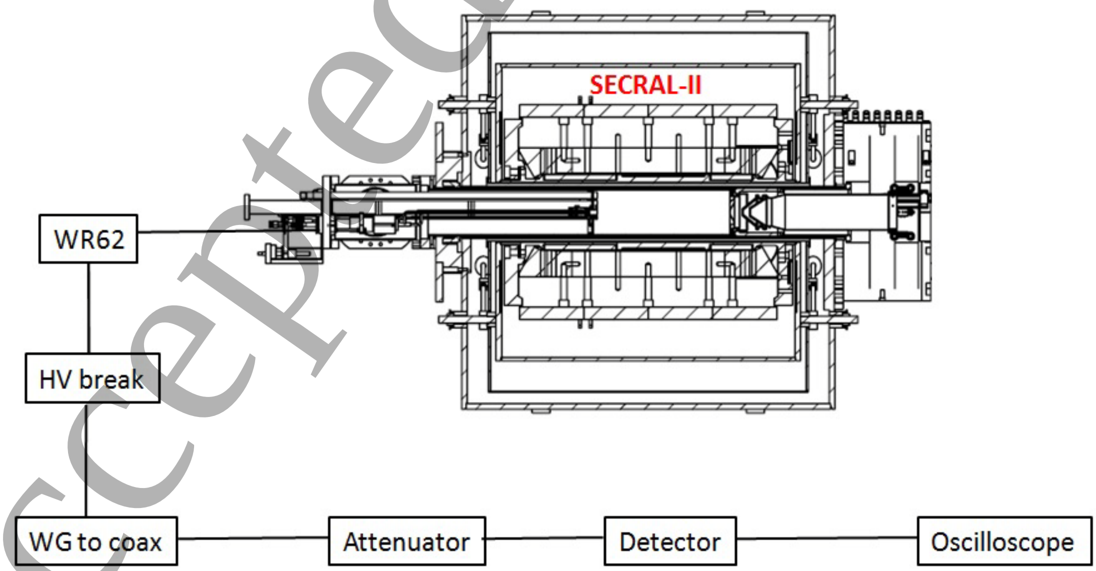

Figure 4: Schematic figure of experimental setup of microwave signal measurement.

The theoretical research shows that electron cyclotron instability is driven by hot electrons interacting resonantly with electromagnetic plasma waves, therefore the emission of microwaves from ECR plasma is a characteristic feature of the electron cyclotron plasma instability as discussed in a recent paper by Shalashov et al. [34] addressing the dynamics of periodic microwave emission and corresponding temporal modulation of the electron energy distribution. Following Refs. [35-38] the energy of the microwave emission E_μ can be described by $\frac{dE_\mu}{dt} \approx (\gamma - \delta) E_\mu$, where γ and δ are mode-dependent growth and damping rates, respectively. Since the growth rate is proportional to the ratio of hot to cold electron densities ($\gamma \propto \frac{N_{e,hot}}{N_{e,cold}}$), and the damping rate is determined by volumetric absorption of the wave energy by the collisional background plasma and external losses ($\delta \propto \nu_e + R$, where R represents the reflection/wall loss term), once the condition $\gamma > \delta$ is reached, the intensity of the microwave emission will increase exponentially with time (usually lasts for about 10-100 ns) as reported e.g. by Izotov et al. [39]. The measurement setup does not allow detecting the emission frequencies associated with the instability. However, it has been shown previously with 14 GHz ECR ion sources that [39, 40] the instability-induced emission frequencies are predominantly lower than the plasma heating frequency. The intensity of the instability-induced microwave burst exceeds the continuous (background) signals of the plasma electron cyclotron emission (ECE) and the primary heating frequency coupled into the diagnostics port by several orders of magnitude. Figure 5 shows a typical microwave signal on SECRAL-II when the electron cyclotron instability is triggered.

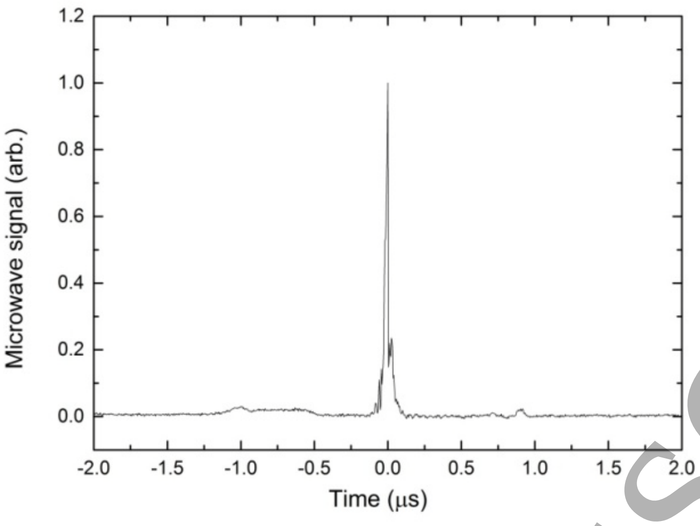

Figure 5: Example of microwave signal associated with the electron cyclotron instability.

3. Experimental results

In all measurements the ion source is operated with xenon plasma and first tuned for Xe^{20+} production. Typical extraction voltage is 20 kV and bias disc voltage is -40-50 V at a power level of 1500 W, data are measured with similar gas pressure of 1-2*10^{-7} mbar. Previous theoretical and experimental studies [25, 41-43] indicate that the minimum magnetic field B_{min} and the gradient parallel to the magnetic field at the resonance zone, $\left|(\vec{B}/|\vec{B}|)\cdot\nabla\vec{B}\right|_{ecr}$, referred hereafter simply as ∇B_{ecr} are the key parameters of the magnetic field configuration and play an important role in magnetically confined ECR plasma, so in the first part of this study, B_{min} is changed while the other fields (B_{inj}, B_{ext} and B_r) are held constant. Figure 6 shows the magnetic field configuration for the 18 and 24 GHz settings. For the 18 GHz case, B_{min} is changed from 0.32 T to 0.52 T with B_{inj}, B_{ext} and B_r at 1.75 T, 1.32 T and 1.20 T, respectively. For the 24 GHz case, similarly, B_{min} is varied from 0.45 T to 0.66 T with fixed B_{inj}, B_{ext} and B_r separately (2.60 T, 1.81 T and 1.66 T). Here, the B_r value is taken in the plane where the radial component of the solenoid field is zero, i.e. B_r represents the hexapole field component. The experimental results in Figure 7 show that the spectral temperature T_s increases almost linearly with the increase of B_{min} for both 18 and 24 GHz heating up to certain values, i.e. 0.51 T and 0.66 T for 18 and 24 GHz, respectively. When B_{min} exceeds the above values, electron cyclotron instabilities are detected and T_s deviates from the increasing trend observed below the instability threshold (this conclusion is supported by additional data presented in Section 4).

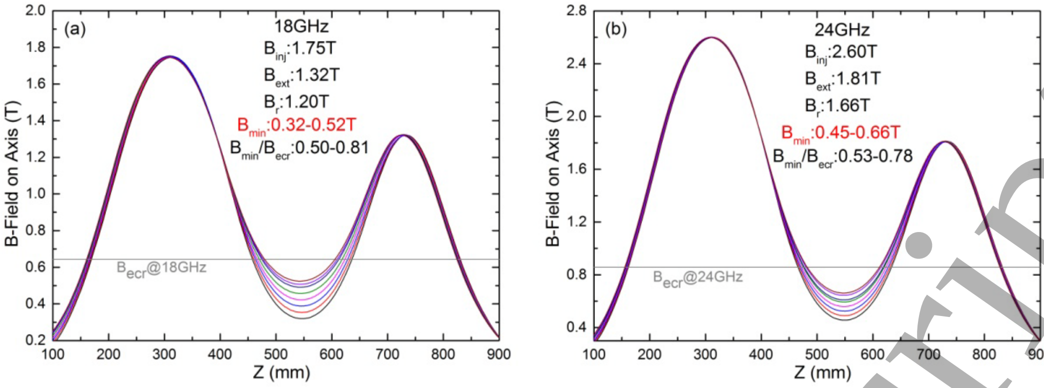

Figure 6: Axial magnetic fields for 18 GHz (a) and 24 GHz (b) heating with constant injection, extraction and radial fields.

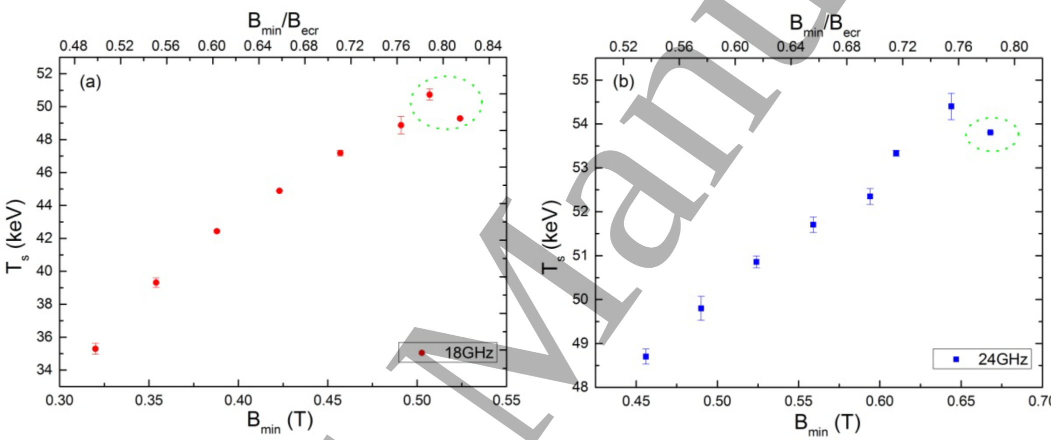

Figure 7: Spectral temperature T_s as a function of B_{min} with constant injection, extraction and radial fields for 18 GHz (a) and 24 GHz (b) heating. The circled data points are the cases where the instabilities are detected.

However, one should note that in these cases when B_{min} is changed, on-axis ∇B_{ecr} is also simultaneously changed. So in the part two of the study, on-axis ∇B_{ecr} is held approximately constant (18 GHz: ~6.3 T/m, 24 GHz: ~9.2 T/m) but B_{min} is changed for the two heating frequencies 18 and 24 GHz (shown in Figure 8). For 18 GHz heating, B_{min} is varied from 0.31 T to 0.47 T with a constant B_r at 1.02 T, the corresponding variations of the injection and extraction fields are 1.13 T to 2.65 T and 1.03 T to 1.68 T, respectively. For 24 GHz, B_{min} is varied from 0.39 T to 0.57 T with a fixed B_r (1.44 T), accordingly, the injection and extraction fields are changed from 1.76 T to 3.43 T and 1.45 T to 2.05 T. It is seen from Figure 9 that when on-axis ∇B_{ecr} is held approximately constant, T_s depends almost linearly on B_{min} for both two heating frequencies. Meanwhile, electron cyclotron instabilities do not appear.

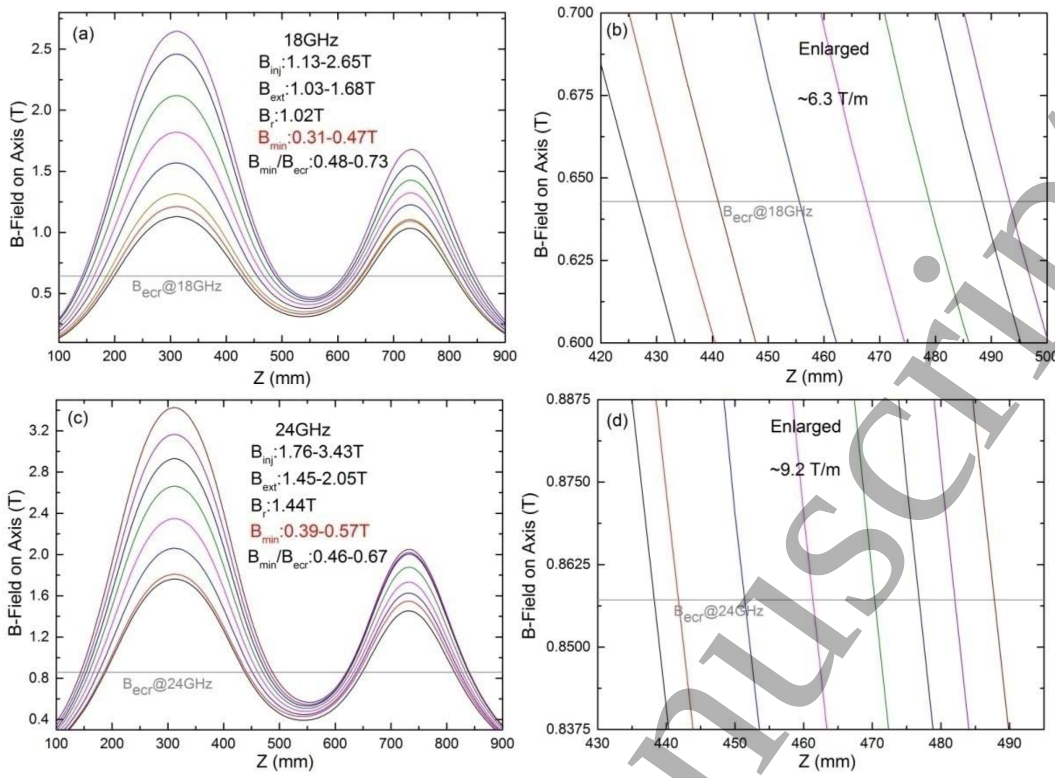

Figure 8: Axial magnetic fields for quasi-constant on-axis ∇B_{ecr} at 18 GHz (a & b) and 24 GHz (c & d) heating.

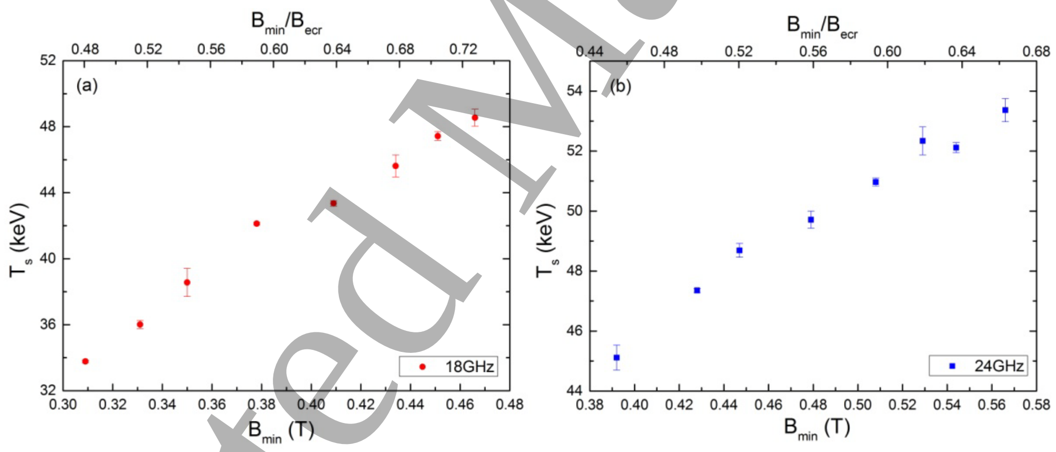

Figure 9: Spectral temperature T_s for 18 (a) and 24 (b) GHz heating at quasi-constant on-axis ∇B_{ecr}.

For comparison, in the third experimental part, B_{min} is kept constant and we vary on-axis ∇B_{ecr} for 18 and 24 GHz (see Figure 10). At 18 GHz, with B_{min} and B_r held constant at 0.40 T and 1.05 T, the injection and extraction fields are varied from 1.06 T to 2.41 T and 1.10 T to 1.50 T. While, at 24 GHz, the injection and extraction fields are varied from 2.12 T to 3.58 T and 1.61 T to 2.14 T corresponding to B_{min} = 0.59 T and B_r = 1.53 T. Figure 11 shows that the resulting T_s decreases with the increase of ∇B_{ecr} at low mirror ratio and is insensitive to the gradient at high mirror ratio for both 18 and 24 GHz heating. Electron cyclotron instabilities are not found at any point in this sweep.

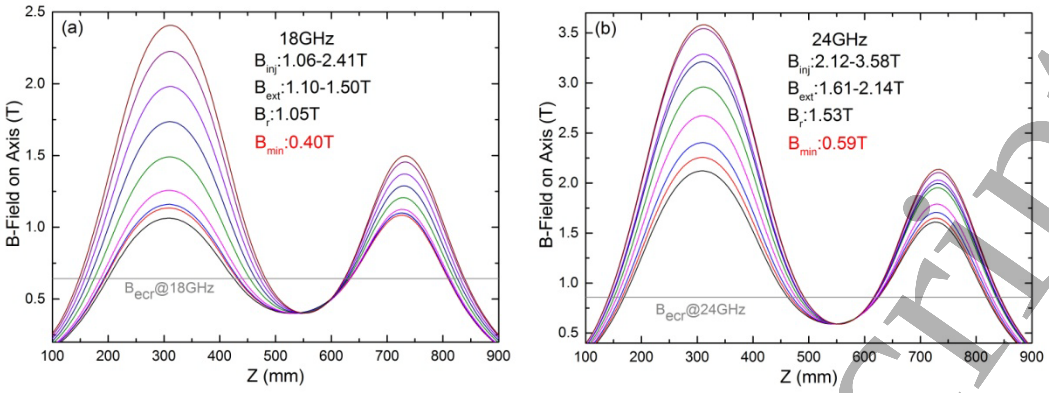

Figure 10: Axial magnetic fields when B_{min} is kept constant (a) at 18 GHz, (b) at 24 GHz.

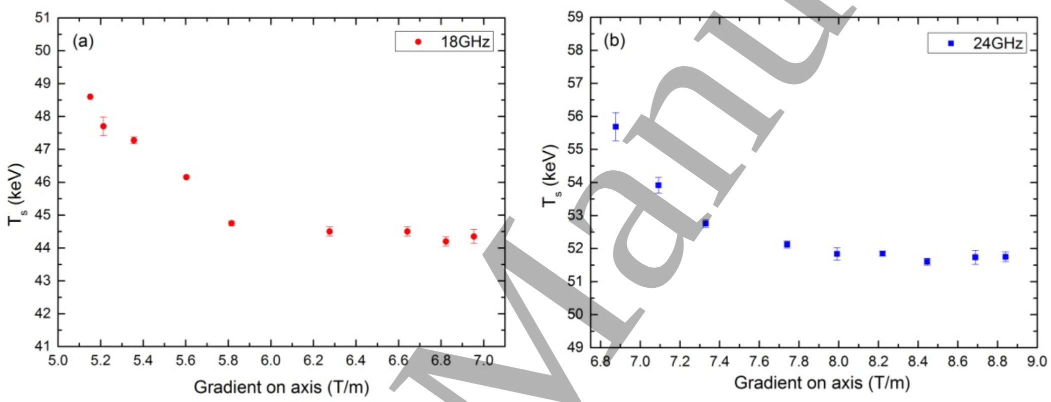

Figure 11: Spectral temperature T_s as a function of on-axis ∇B_{ecr} for 18 (a) and 24 (b) GHz heating with constant B_{min}.

Since the increase of the axial mirror fields (and on-axis gradient at constant B_{min}) changes the radial component of the solenoid field and, thus, affects the strength of the radial confinement by weakening the hexapole field on three poles in the injection side and on the other three poles in the extraction side, the effect of the radial field on T_s was also investigated. In this sweep, carried out with 24 GHz frequency, the on-axis gradient (8.1 T/m) and B_{min} (0.60 T) as well as the injection and extraction mirror fields (3.00 T and 1.98 T) were kept constant. The result is displayed in Figure 12 showing that T_s is affected by the radial field strength.

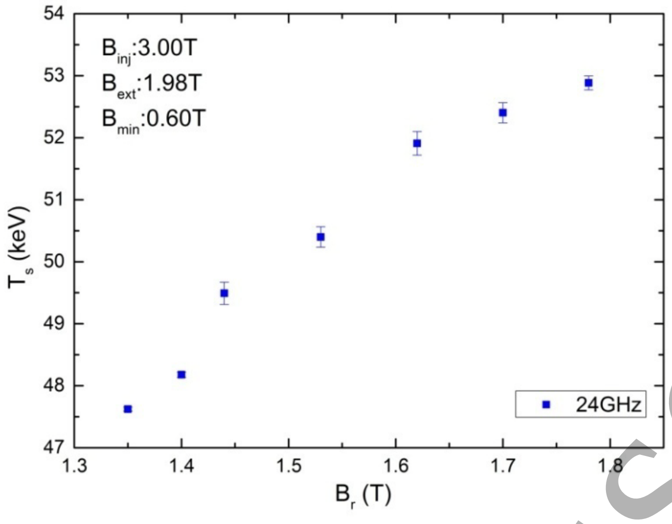

Figure 12: Spectral temperature T_s as a function of B_r. Here B_r is measured in the plane where the radial component of the solenoid field does not affect the hexapole field.

4. Discussion

The experimental results obtained in part one indicate that electron cyclotron instability appears above a threshold B_{min}, which gave us a hint to extend the B_{min} range. Figure 13 presents the summary of T_s versus extended B_{min}/B_{ecr} for two heating frequencies powered separately (18 and 24 GHz) at various magnetic field configurations. It can be seen from this figure that T_s increases approximately linearly with the increasing of B_{min}/B_{ecr} but deviates from this trend (appears to saturate) above a threshold (18 GHz: ~0.79, 24 GHz: ~0.78), i.e. in the regime where electron cyclotron instabilities are detected. This phenomenon can be explained by the fact that the spectral temperature T_s is determined by the hot electron population, and electron cyclotron instabilities would expel a significant fraction of the hot electrons into the loss cone [21]. Once the electron cyclotron instabilities are triggered, the plasma energy content (affected predominantly by the hot electrons) starts to oscillate around a certain average value [34], which is then observed as a saturation of the bremsstrahlung spectral temperature averaged over a large number of instability periods. This finding is also consistent with experimental study [33] on the energy distribution of electrons escaping minimum-B ECR plasmas, it is demonstrated that the average energy of electrons escaping axially from a minimum-B ECRIS grows with the magnetic field up to $B_{min}/B_{ecr} \sim 0.8$ and then saturates.

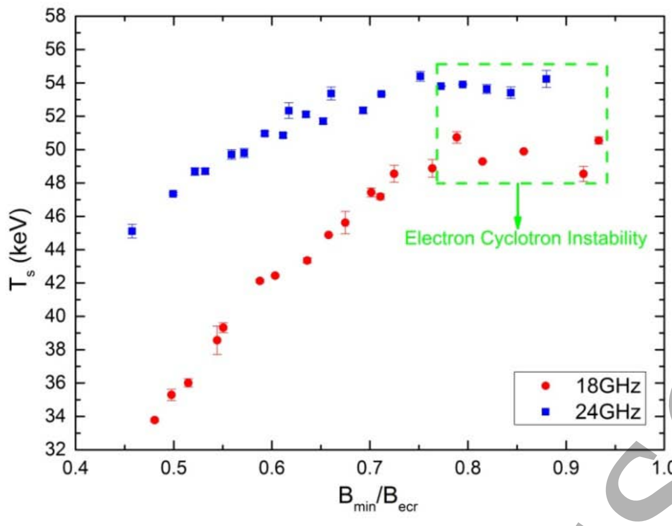

Figure 13: Spectral temperature T_s as a function of B_{min}/B_{ecr}.

Regarding part two, since B_{min} is not directly linked with the electron energy gain in single resonance crossing, conversely, the electron energy gain depends strongly on the magnetic field gradient at the resonance [41, 42]. Furthermore, the effective width of the resonance also depends on the component of the magnetic field gradient [43]. Although the spectral temperature T_s in our experiments is determined by the bremsstrahlung emitted by the electrons near the source axis and the gradient on axis is held approximately constant, one should note that the ECR heating of cold electrons takes place over the whole ECR surface for which the above parameters have been calculated. For relativistic electrons producing bremsstrahlung in the range of 80–200 keV (used for determining T_s) the situation is far more complicated as they are heated everywhere in the discharge volume where the Doppler shifted relativistic resonance condition $B_{\mathrm{ecr}} = \frac{1}{n} B_{ecr,cold}\, \gamma\left(1 \pm N_{||} k_{||}\right)$ is met. Here n is the harmonic number, γ the relativistic Lorentz gamma ($\gamma = 1 + \frac{E_k}{m_e c^2}$), $N_{||} k_{||} = \frac{v_{e,||}}{v_{\varphi}}$ the ratio of electron longitudinal velocity (with respect to the propagating wave) and the phase velocity of the heating microwave and the $\pm$ sign corresponds to blue- and red-shifted resonances. Hence, it should not be the on-axis gradient, which is commonly used [13, 25, 27] as a parameter to describe the magnetic field configuration of an ECRIS, but rather a global effect that determines the electron heating rate and the bremsstrahlung spectrum. In fact, there is no single parameter that could be used to describe the relativistic electron heating efficiency in Doppler-shifted resonance. In the following we will use the average gradient $<\nabla B_{ecr}> = \langle \left(\left(\vec{B}/|\vec{B}| \right) \cdot \nabla \vec{B} \right)_{ecr,cold} \rangle$ (parallel to the field lines) across the cold electron resonance surface to describe each configuration. This is preferred over the on-axis cold electron resonance gradients because the variation of $<\nabla B_{ecr}>$ is proportional to the variation of the average gradient in the whole discharge volume where the Doppler-shifted resonance can occur.

Table 1 and figure 14 show that for 18 GHz heating of part two, the calculated [44] $<\nabla B_{ecr}>$ decreases with the increase of B_{min} and accordingly T_s decreases linearly with the increase of $<\nabla B_{ecr}>$. This consequence also applies for those cases in part one and can be used to explain the appearance of electron cyclotron instabilities: since the growth rate of electron cyclotron instabilities is proportional to the ratio of hot and cold electron densities ($\gamma \propto \frac{N_{e,hot}}{N_{e,cold}}$), when increasing B_{min} while keeping the other fields constant, decreasing average gradient over ECR surface (shown in Figure 15) will lead to an increase in the hot electron population due to the more efficient heating process. In other words, it means that the growth rate of electron cyclotron instabilities increases with the increase of B_{min}. This process will continue until the condition that the growth rate is larger than damping rate ($\gamma > \delta$) is reached, then the electron cyclotron instabilities are triggered and T_s stops increasing. It is important to note that both the instability growth and damping rates most likely depend on the magnetic field configuration through the electron energy distribution and varying plasma density and electron loss rates. However, we associate the transition between the stable and unstable regimes with the increase of the instability growth rate rather than the decrease of the damping rate as it has been shown previously that [19] the magnetic field is more influential than the neutral gas pressure (affecting the plasma density) in determining the transition. Based on the above analyses, it may be argued that separating the effect of B_{min} from the effect of $<\nabla B_{ecr}>$ is problematic while considering on the role of average gradient is more coincident with theoretical studies to explain the apparent B_{min} dependence.

Table 1: Ion source characteristics for the study of the average gradient influence on T_s.

f (GHz)	B_r (T)	B_{inj} (T)	B_{min} (T)	B_{ext} (T)	$<\nabla B_{ecr}>$ (T/m)	T_s (keV)
18	1.02	1.13	0.31	1.03	8.74	33.8
		1.21	0.33	1.09	8.38	36.1
		1.32	0.35	1.11	7.97	38.6
		1.57	0.38	1.23	7.67	42.1
		1.82	0.41	1.32	7.17	43.4
		2.12	0.43	1.43	6.79	45.6
		2.46	0.45	1.55	6.62	47.4
		2.65	0.47	1.68	6.32	48.6

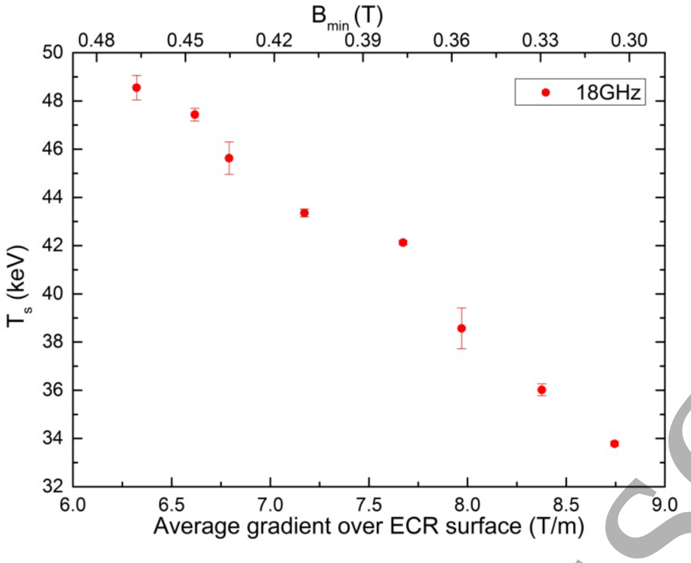

Figure 14: Spectral temperature T_s as a function of the average gradient over ECR surface.

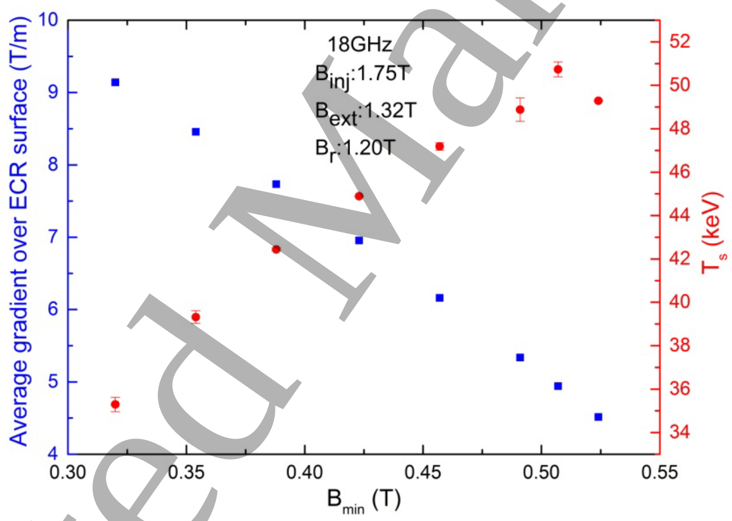

Figure 15: The average gradient over ECR surface and spectral temperature T_s as a function of B_{min}.

For the constant B_{min} cases in part three, similarly, we also take into account the influence of average gradient over ECR surface, it is found that for the 18 GHz heating, both ∇B_{ecr} on axis and $<\nabla B_{ecr}>$ increase with increasing of mirror ratio (see Table 2), hence the changing trend of T_s for these two parameters are the same (shown in Figure 16). It should be noted that in this setting of experiments, when B_{min} is kept constant, the changes of gradient (∇B_{ecr} on axis: 5.15 – 6.95 T/m; $<\nabla B_{ecr}>$: 6.92 – 7.70 T/m) and mirror ratio (B_{max}/B_{min}: 2.65 – 6.03) occur simultaneously, which means that two processes, i.e. electron heating and electron confinement are changed simultaneously.

Table 2: Ion source characteristics for the study of constant B_{min} cases of 18GHz heating.

f (GHz)	B_r (T)	B_{min} (T)	B_{inj} (T)	B_{ext} (T)	∇B_{ecr} on axis (T/m)	$<\nabla B_{ecr}>$ (T/m)
18	1.05	0.40	1.06	1.10	5.15	6.92
			1.14	1.11	5.21	6.95
			1.16	1.12	5.36	6.98
			1.26	1.13	5.60	7.05
			1.49	1.21	5.82	7.13
			1.74	1.29	6.28	7.31
			1.98	1.37	6.64	7.43
			2.23	1.45	6.82	7.57
			2.41	1.50	6.95	7.70

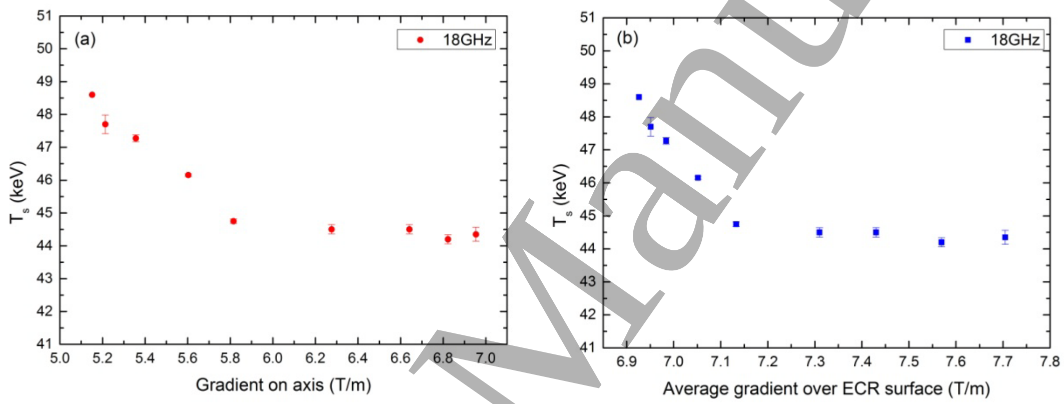

Figure 16: Spectral temperature T_s as a function of gradient on axis (a) and the average gradient over ECR surface (b).

The data in Figure 16 shows that the effect of the average gradient on T_s becomes weaker when $<\nabla B_{ecr}>$ increases, which implies that the electron heating rate alone does not define T_s. This assumption is supported by the influence of B_r on T_s: figure 12 shows that T_s increases with the increase of B_r when the axial magnetic fields are held constant. At the same time the average gradient on the ECR-surface is affected only weakly as shown in Table 3 where the magnetic field strength B_{last} defining the last closed surface takes into account the effect of the radial component of the solenoid field on the hexapole (radial field). Since B_{last} defines the overall magnetic confinement in ECR plasma [13], the result implies that T_s is affected by the electron confinement, not only by electron heating. This conclusion is corroborated by the fact that both, the bremsstrahlung count rate and maximum energy, were observed to increase with the radial field strength (last closed surface).

Table 3: Ion source characteristics for the study of the radial field.

f (GHz)	B_{inj} (T)	B_{min} (T)	B_{ext} (T)	B_r (T)	$<\nabla B_{ecr}>$ (T/m)	B_{last} (T)
24	3.00	0.60	1.98	1.35	9.09	1.05
				1.40	9.13	1.09
				1.44	9.18	1.13
				1.53	9.29	1.21
				1.62	9.39	1.29
				1.70	9.50	1.37
				1.78	9.61	1.45

5. Conclusion

The experimental results of this study show for the first time that the bremsstrahlung spectral temperature T_s increases approximately linearly with the increase of B_{min}/B_{ecr} up to ~ 0.8 and then saturates with the appearance of electron cyclotron instabilities. Based on the earlier analyses in this paper, it is suggested that once the electron cyclotron instabilities are triggered, periodic bursts of energetic electrons escaping the magnetic confinement will limit the increase of the energy content carried by the hot electron population and eventually lead to a saturation of T_s.

Previous studies have typically used either the B_{min} or the on-axis gradient as the only parameter to explain the dependence of T_s on the magnetic configuration. However, as discussed above, B_{min} is not directly linked with the electron energy gain and the on-axis gradient does not reflect the global effect of ECR heating. This study is the first attempt to demonstrate that increasing B_{min} corresponds to decreasing average (parallel) gradient over the ECR surface although the on-axis gradient remains constant, which shows the inherent link between B_{min} and average gradient over the ECR surface, and thus provides a viewpoint that is more coincident with theoretical studies to understand the apparent linear B_{min} dependence and the appearance of electron cyclotron instabilities.

In this study, it also has been shown that T_s decreases with the increasing of gradient (∇B_{ecr} on axis and $<\nabla B_{ecr}>$) at relatively low mirror ratio and is insensitive to the gradient at high mirror ratio when B_{min} is constant, which indicates that T_s depends on not only electron heating, but also depends on electron confinement. This view is supported by the dependence of T_s on the radial confinement. The conclusion is different from the one made in Ref. [25] where the radial field was kept constant and then argued that the T_s depends only on B_{min}.

Acknowledgments

The authors wish to thank J. Benitez and D. Xie of LBNL for helpful discussions. This work has been funded by Chinese Academy of Sciences President's International Fellowship Initiative (Grant No. 2016VTA009) and supported by the NSFC (contract No. 11427904), CAS (contract No. QYZDB-SSW-JSC025) and NSFC (contract No.

11705254).

References

[1] Geller R 1996 *Electron cyclotron resonance ion sources and ECR plasmas* (Bristol: Institute of Physics Publishing)

[2] Geller R 1998 *Rev. Sci. Instrum.* **69** 1302-10

[3] Liu Z W et al. 1998 *Rev. Sci. Instrum.* **69** 685-87

[4] Zhao H W, Wei B W, Liu Z W, Wang Y F and Zhao W J 2000 *Rev. Sci. Instrum.* **71** 646-50

[5] Zhao H W et al. 2002 *Rev. Sci. Instrum.* **73** 525-27

[6] Zhao H W et al. 2004 *Rev. Sci. Instrum.* **75** 1410-13

[7] Zhao H W et al. 2008 *Rev. Sci. Instrum.* **79** 02A315

[8] Lu W et al. 2016 *Rev. Sci. Instrum.* **87** 02A738

[9] Sun L et al. 2016 *Rev. Sci. Instrum.* **87** 02A707

[10] Zhao H W et al. 2018 *Rev. Sci. Instrum.* **89** 052301

[11] Zhao H Y et al. 2006 *Rev. Sci. Instrum.* **77** 03A312

[12] Zhao H Y et al. 2008 *Rev. Sci. Instrum.* **79** 02B504

[13] Zhao H Y et al. 2009 *Plasma Sources Sci. Technol.* **18** 025021

[14]Guo J W, Sun L, Niu X J, Zhang X Z, Lu W, Zhang W H, Feng Y C and Zhao H W 2016 *Rev. Sci. Instrum.* **87** 02A708

[15] Guo J W et al. 2018 *AIP Conference Proceedings* **2011** 090001

[16] Sun L et al. 2018 *AIP Conference Proceedings* **2011** 040022

[17] Lyneis C, Leitner D, Todd D, Virostek S, Loew T, Heinen A and Tarvainen O 2006 *Rev. Sci. Instrum.* **77** 03A342

[18] Thuillier T, Angot J, Benitez J Y, Hodgkinson A, Lyneis C M, Todd D S and Xie D Z 2016 *Rev. Sci. Instrum.* **87** 02A736

[19] Tarvainen O et al. 2014 *Plasma Sources Sci. Technol.* **23** 025020

[20] Tarvainen O, Laulainen J, Komppula J, Kronholm R, Kalvas T, Koivisto H, Izotov I, Mansfeld D and Skalyga V 2015 *Rev. Sci. Instrum.* **86** 023301

[21] Tarvainen O et al. 2016 *Rev. Sci. Instrum.* **87** 02A703

[22] Barue C, Briand P, Girard A, Melin G and Briffod G 1992 *Rev. Sci. Instrum.* **63** 2844-46

[23] Girard A 1992 *Rev. Sci. Instrum.* **63** 2676-82

[24] Baskaran R, Selvakurnaran T S, Rodrigues G, Kanjilal D and Roy A 2008 *Rev. Sci. Instrum.* **79** 02A324

[25] Benitez J, Lyneis C, Phair L, Todd D and Xie D 2017 *IEEE Trans. Plasma Sci.* **45** 1746-54

[26] Leitner D, Benitez J Y, Lyneis C M, Todd D S, Ropponen T, Ropponen J, Koivisto H and Gammino S 2008 *Rev. Sci. Instrum.* **79** 033302

[27] Noland J, Tarvainen O, Benitez J, Leitner D, Lyneis C and Verboncoeur J 2011 *Plasma Sources Sci. Technol.* **20** 035022

[28] Sun L et al. 2020 *Rev. Sci. Instrum.* **91** 023310

[29] http://amptek.com/products/xr-100cdte-x-ray-and-gamma-ray-detector/

[30] Bernhardi K and Wiesemann K 1982 *Plasma Phys. Controlled Fusion* **24** 867-84

[31] X-5 Monte Carlo Team 2003 *MCNP- A General Monte Carlo N-Particle Transport Code, Version 5* (NM: Los Alamos National Laboratory)

[32] Perret C, Girard A, Khodja H and Melin G 1999 *Physics of Plasmas* **6** 3408-15

[33] Izotov I, Tarvainen O, Skalyga V, Mansfeld D, Kalvas T, Koivisto H and Kronholm R 2018 *Plasma Sources Sci. Technol.* **27** 025012

[34] Shalashov A G, Gospodchikov E D, Izotov I V, Mansfeld D A, Skalyga V A and Tarvainen O 2018 *Epl* **124** 35001

[35] Ginzburg V L 1970 *The propagation of electromagnetic waves in plasmas* (Oxford: Pergamon Press)

[36] Golubev S V and Shalashov A G 2007 *Phys. Rev. Lett.* **99** 205002

[37] Golubev S V and Shalashov A G 2007 *JETP Lett.* **86** 91-97

[38] Trakhtengerts V Y and Rycroft M J 2008 *Whistler and Alfven mode cyclotron masers in space* (Cambridge: Cambridge University Press)

[39] Izotov I, Tarvainen O, Mansfeld D, Skalyga V, Koivisto H, Kalvas T, Komppula J, Kronholm R and Laulainen J 2015 *Plasma Sources Sci. Technol.* **24** 045017

[40] Naselli E et al. 2019 *Plasma Sources Sci. Technol.* **28** 085021

[41] Canobbio E 1969 *Nucl. Fusion* **9** 27-47

[42] Gammino S, Mascali D, Celona L, Maimone F and Ciavola G 2009 *Plasma Sources Sci. Technol.* **18** 045016

[43] Williamson M C, Lichtenberg A J and Lieberman M A 1992 *J. Appl. Phys.* **72** 3924-33

[44] Vaughan J R M 1972 *IEEE Trans. Electron Devices* **Ed19** 144-151